LAWRENCE
LIVERMORE
NATIONAL
LABORATORY

UCRL-JRNL-225231

Mineralogy and Petrology of Comet Wild 2 Nucleus Samples

M. E. Zolensky, T. J. Zega, H. Yano, S. Wirick, A. J. Westphal, M. K. Weisberg, I. Weber, J. L. Warren, M. A. Velbel, A. Tsuchiyama, P. Tsou, A. Toppani, N. Tomioka, K. Tomeoka, N. Teslich, M. Taheri, J. Susini, R. Stroud, T. Stephan, F. J. Stadermann, C. J. Snead, S. B. Simon, A. Siminovici, T. H. See, F. Robert, F. J. M. Rietmeijer, W. Rao, M. C. Perronnet, D. A. Papanastassiou, K. Okudaira, K. Ohsumi, I. Ohnishi, K. Nakanura-Messenger, T. Nakamura, S. Mostefaoui, T. Mikouchi, A. Meibom, G. Matrajt, M. A. Marcus, H. Leroux, L. Lemelle, L. Le, A. Lanzirotti, F. Langenhorst, A. N. Krot, L. P. Keller, A. T. Kearsley, D. Joswiak, D. Jacob, H. Ishii, R. Harvey, K. Hagiya, L. Grossman, G. A. Graham, M. Gounelle, P. Gillet, M. J. Genge, G. Flynn, T. Ferrior, et al.

October 11, 2006

Science

Mineralogy and Petrology of Comet Wild 2 Nucleus Samples

Michael E. Zolensky[1*], Thomas J. Zega[2], Hajime Yano[3], Sue Wirick[4], Andrew J. Westphal[5], Mike K. Weisberg[6], Iris Weber[7], Jack L. Warren[8], Michael A. Velbel[9], Akira Tsuchiyama[10], Peter Tsou[11], Alice Toppani[12,13], Naotaka Tomioka[14], Kazushige Tomeoka[14], Nick Teslich[12], Mitra Taheri[2], Jean Susini[15], Rhonda Stroud[2], Thomas Stephan[7], Frank J. Stadermann[16], Christopher J. Snead[5], Steven B. Simon[17], Alexandre Simionovici[18], Thomas H. See[19], François Robert[20], Frans J.M. Rietmeijer[21], William Rao[22], Murielle C. Perronnet[1], Dimitri A. Papanastassiou[23], Kyoko Okudaira[3], Kazumasa Ohsumi[24], Ichiro Ohnishi[14], Keiko Nakamura-Messenger[8], Tomoki Nakamura[25], Smail Mostefaoui[20], Takashi Mikouchi[26], Anders Meibom[20], Graciela Matrajt[27], Matthew A. Marcus[28], Hugues Leroux[29], Laurence Lemelle[18], Loan Le[8], Antonio Lanzirotti[30], Falko Langenhorst[31], Alexander N. Krot[32], Lindsay P. Keller[1], Anton T. Kearsley[33], David Joswiak[27], Damien Jacob[29], Hope Ishii[12], Ralph Harvey[34], Kenji Hagiya[35], Lawrence Grossman[17,36], Jeffrey N. Grossman[37], Giles A. Graham[12], Matthieu Gounelle[20,33], Philippe Gillet[18], Matthew J. Genge[38], George Flynn[39], Tristan Ferroir[18], Stewart Fallon[12], Denton S. Ebel[40], Zu Rong Dai[12], Patrick Cordier[29], Miaofang Chi[12], Anna L. Butterworth[5], Donald E. Brownlee[27], John C. Bridges[41], Sean Brennan[42], Adrian Brearley[21], John P. Bradley[12], Pierre Bleuet[15], Phil A. Bland[33,38], and Ron Bastien[8]

[1]Astromaterials Research and Exploration Science, NASA Johnson Space Center, Houston, Texas 77058, USA.

[2]Code 6360, Naval Research Laboratory, 4555 Overlook Ave. SW, Washington, DC 20375, USA

[3]JAXA-ISAS, 3-1-1 Yoshinodai, Sagamihara, Kanagawa, 229-8510 Japan

[4]National Synchrotron Light Source, Brookhaven National Lab, Upton, NY 11973, USA

[5]Space Sciences Laboratory, University of California, 7 Gauss Way, Berkeley, CA 94720-7450, USA

[6]Physical Sciences, Kingsborough Community College (CUNY), Brooklyn, NY 11235, USA

[7]Institut für Planetologie, Westfälische Wilhelms-Universität Münster, Wilhelm-Klemm-Str.10, 48149 Münster, Germany

[8]Jacobs Sverdrup, ESCG, Houston, TX 77058, USA

[9]Department of Geological Sciences, 206 Natural Science Building, Michigan State University, East Lansing, MI 48824-1115, USA

[10]Department of Earth and Space Science, Osaka University, 1-1 Machikaneyama-cho, Toyonaka, 560-0043, Japan

[11]Jet Propulsion Laboratory, M/S 183-501, 4800 Oak Grove Drive, Pasadena, CA 91109 USA

[12]Institute for Geophysics and Planetary Physics, Lawrence Livermore National Laboratory, Livermore, CA 94550, USA

[13]Centre de Spectrometrie Nucleaire et de Spectrometrie de Masse, Bat 104, 91405 Orsay Campus, France

[14]Department of Earth and Planetary Sciences, Faculty of Science, Kobe University, Nada, Kobe 657-8501, Japan

[15]European Synchrotron Radiation Facility, BP 220, 38043 Grenoble, France

[16]Department of Physics, Washington University, St. Louis, MO 63130 USA

[17]Department of the Geophysical Sciences, The University of Chicago, 5734 S. Ellis Ave., Chicago, IL 60637 USA

[18]Laboratoire de Sciences de la Terre, Ecole Normale Superieure de Lyon, 46, allee d'Italie, 69007, Lyon, France

[19]ESC/Barrios Technology, ARES/JSC, Houston, Texas 77258-8447, USA

[20]Museum National d'Histoire Naturelle, Laboratoire d'Etude de la Matiere Extraterrestre, USM 0205 (LEME), Case Postale 52, 57, rue Cuvier, 75005 Paris, France

[21] Department of Earth and Planetary Sciences, University of New Mexico, MSC 03-2040, Albuquerque, NM 87131-0001, USA

[22]Savannah River Ecology Lab, Aiken, SC 29801, USA

[23]Science Division, Jet Propulsion Laboratory, M/S 183-335, 4800 Oak Grove Dr., Pasadena, CA 91109, USA

[24]Institute of Materials Structure Science, Tsukuba-shi, Ibaraki-ken, 305, Japan

[25]Department of Earth and Planetary Sciences Faculty of Sciences Kyushu University Hakozaki, Fukuoka 812-8581, Japan

[26]Department of Earth and Planetary Science, University of Tokyo, Hongo, Bunkyo-ku, Tokyo 113-0033, Japan

[27]Department of Astronomy, University of Washington, Seattle, WA 98195, USA

[28]Advanced Light Source, Lawrence Berkeley National Lab, 1 Cyclotron Road MS 2R2100, Berkeley, CA 94720, USA

[29]Laboratoire de Structure et Propriétés de l'Etat Solide, Bat C6, Université des Sciences et Technologies de Lille, 59655 Villeneuve d'Ascq, France

[30]Consortium for Advanced Radiation Sources, The University of Chicago, Chicago, IL, 60637, USA

[31]Institute of Geosciences, Friedrich-Schiller-University Jena, Burgweg 11, D-07749 Jena, Germany

[32]Hawaii Institute of Geophysics and Planetology, University of Hawaii, Honolulu, HI 96822, USA

[33]Department of Mineralogy, Natural History Museum, Cromwell Road, London, SW7 5BD, UK

[34]Geology Department, Case Western Reserve University, Cleveland, OH 44106, USA

[35]Graduate School of Life Science, University of Hyogo, Koto 3-2-1, Kamigori, Ako-gun, Hyogo 678-1297, Japan

[36]Enrico Fermi Institute, The University of Chicago, 5640 S. Ellis Ave., Chicago, IL 60637, USA

[37]United States Geological Survey, 954 National Center, Reston, VA 20192, USA

[38]Impact and Astromaterials Research Centre, Department of Earth Sciences and Engineering, Imperial College of Science Technology and Medicine, Prince Consort Road, London, SW7 2AZ, UK

[39]Department of Physics, SUNY, Plattsburgh NY 12901 USA

[40]Dept. Earth and Planetary Sciences, American Museum of Natural History, Central Park West at 79th Street, New York, NY 10024, USA

[41]Planetary and Space Sciences Research Institute, Open University, Milton Keynes, MK7 6AA, UK

[42]Stanford Linear Accelerator Center, Menlo Park, CA 94025, USA.

* to whom correspondence should be addressed; E-mail: michael.e.zolensky@ nasa.gov

The bulk of the Wild 2 samples appear to be weakly-constructed mixtures of nanometer-scale grains with occasional much larger (>1μm) ferromagnesian silicates, Fe-Ni sulfides, Fe-Ni metal and accessory phases. The very wide range of olivine and low-Ca pyroxene compositions in Wild 2 require a wide range of formation conditions, probably reflecting different formation locations in the protoplanetary disk. The restricted compositional ranges of Fe-Ni sulfides, the wide range for silicates, and absence of hydrous phases indicate that Wild 2 experienced little or no aqueous alteration. Less abundant Wild 2 materials include a refractory particle, whose presence appears to require large-scale radial transport in the early protoplanetary disk.

The nature of cometary solids is of fundamental importance to our understanding of the early solar nebula and protoplanetary history. Until now we have had to study comets from afar using spectroscopy, or settle for analyses of interplanetary dust particles (IDPs) of uncertain provenance. We report here mineralogical and petrographic analyses of particles derived directly from Comet Wild 2.

All of the Wild 2 particles we have thus far examined have been modified in various ways by the capture process. All particles that may have been loose aggregates, "traveling sand piles", disaggregated into individual components with the larger, denser components penetrating more deeply into the aerogel. Individual grains experienced a wide range of heating effects that range from excellent preservation to melting (Fig. 1); such behavior was expected (1, 2 ,3). What is remarkable is the extreme variability of these modifications and the fact that severely modified and unmodified materials can be found within a micrometer of each other, requiring tremendous local temperature gradients. Fortunately, we have an internal gauge of impact collection heating. Fe-Ni sulfides are ubiquitous in the Wild 2 samples, are very sensitive

indicators of heating, and accurate chemical analyses can reveal which have lost S, and which have not (and are therefore stoichiometric) (Fig. 2). Our surveys show that crystalline grains are found along the entire lengths of tracks, not just at track termini (Fig. S1).

There appears to be very limited contamination from the spacecraft in the aerogel. Potential problems with secondary impacts (cometary grains impacting on the spacecraft, ricocheting and splashing onto the aerogel) failed to materialize. These issues are treated at greater length in the Supplementary Online Material.

We have harvested samples from 52 tracks, and have obtained a significant understanding of the mineralogy of 25 of these. Analyses have also been performed on impact residues in seven aluminum foil craters of greater than 50 μm diameter, and over 200 craters of less than 5 μm (4). Crystalline materials are abundant in Comet Wild 2 and many are "coarse-grained" when considered relative to the submicrometer scales characteristic of many anhydrous IDPs and also inferred for interstellar dust populations (5). Of the best studied 25 tracks, 8 are dominated by olivine grains, 5 by low-calcium pyroxene, 2 by a fairly equal amount of olivine and pyroxene, and the remaining 10 are dominated by other minerals, mainly Fe-Ni sulfides. One of the latter tracks contains predominantly refractory minerals, one contains Na-silicate minerals, and 2 are dominated by ~5 μm-sized Fe sulfide grains. These findings suggest that crystalline materials are abundant in Wild 2.

In the 7 large craters in aluminum foil that we examined, 1 contains only remnants of stoichiometric olivine, 3 are dominated by Mg-silicates and sulfide, and 2 contain a mixture of mafic silicates and Na- and Ca-rich silicates. The last, complex, impact feature has overlapped bowl-shaped depressions containing residues with a heterogeneous collection of stoichiometric compositions suggesting impact by an aggregate of micrometer-scale grains of Ca-rich

clinopyroxene, Mg-rich pyroxene (probably enstatite) and a mixture of Fe Ni sulfides, as well as grains composed of finely-mixed silicate and sulfide. Just over half of the very small craters we examined contain mixtures of silicate and sulfur-bearing residue, while the others are mainly monomineralic olivine, pyroxene and Fe-Ni sulfides, with occasional preservation of crystalline material.

Olivine, one of the most abundant minerals in the solar system (6, 7, 8), is present in the majority of Wild 2 particles. Its observed grain size ranges from submicrometer to over 10 μm. Wild 2 olivine has an extremely wide compositional range, from $Fo_{4\text{-}100}$ (Fo being a measure of the Mg/(Mg+Fe) ratio) (Fig. 3), with a pronounced frequency peak at Fo_{99}. Although it is possible that collection effects have biased surviving olivines to the most refractory, Mg-rich compositions, the abundance of Fe-rich olivine among the Wild 2 samples suggests that this effect has been minor. One olivine crystal in Track 22 was found to display dramatic reverse chemical zoning – from Fo_{70} core to Fo_{92} rim. It is clear that these grains have not been equilibrated during capture, as we would then observe a greatly reduced compositional range and a peak at a high Fe (low Fo) concentration (1, 2, 9, 10).

Wild 2 olivines include varieties with very elevated MnO, Al_2O_3 and Cr_2O_3 contents, up to 6.45, 0.71 and 1.46 wt%, respectively. About 25% of these Mn- and Cr-rich olivines contain <<1% FeO. Olivines with enrichments in these elements have been reported in carbonaceous chondrites, micrometeorites, and chondritic interplanetary dust particles, though they are very rare (11, 12, 13, 14, 15). The compositions of the Mn- and Cr-rich olivines in the Wild 2 samples are similar to those in IDPs, carbonaceous chondrites and unequilibrated ordinary chondrites (Fig. S2). Many Wild 2 olivines contain inclusions of other phases, notably Fe-Cr-Ti oxides (including chromite), but thus far melt inclusions have not been observed within any

silicates. Olivine with low Fe and elevated Mn has been proposed to form from condensation in the protosolar nebula (11).

Wild 2 olivine-dominated grains are commonly polycrystalline, with some interstitial glass, which could be indigenous cometary glass. One fragment from the wall of the 1 cm-long Track 35 was investigated by micro-tomography (16) and found to have a microporphyritic texture with olivine crystals (~Fo_{80}) set within lower density fine-grained material, probably glass. From the manner in which the enclosing aerogel wraps around this particular grain without intruding into it, the glass appears to be indigenous. This fragment has an obvious igneous origin, and resembles a microporphyritic chondrule.

Both low- and high-calcium pyroxenes are present among the Wild 2 grains, with the former being dominant. In some cases Synchrotron X-ray Diffraction (SXRD) or Selected Area Electron Diffraction (SAED) patterns reveal low-calcium pyroxenes to be orthoenstatite, requiring slow cooling (17), but in the majority of cases we have only EDX analyses and are not certain whether we have ortho- or clinopyroxene. The compositional range displayed by the low-calcium pyroxene is also very extensive, from En_{52-100}, with a significant frequency peak centered at En_{95} (Fig. 3). Low-calcium pyroxene usually coexists with olivine, but the Mg/Fe ratios for coexisting phases are not always similar. Track 17 contains olivine in the range Fo_{55-69}, while associated low-calcium pyroxene is En_{52-96}. Flash heating during sample collection may account for this disparity, as olivine equilibrates faster than orthopyroxene under identical circumstances (18). Diopside occurs in several grains usually in association with low-calcium pyroxene. A Ti-, Al-rich diopside is abundant within the CAI-like particle (see below).

Sulfides are the only mineral group found in all extraterrestrial materials. Fe-Ni sulfides are also ubiquitous in the Wild 2 grains, grading from sulfides apparently melted and mixed with

Fe-Ni metal, all the way to apparently unmodified FeS and pentlandite ($(Fe,Ni)_9S_8$) grains (Fig. S3). Several tracks (e.g. Track 59) have FeS- or pentlandite-dominated terminal grains. In this paper we collectively refer to troilite (stoichiometric FeS) and pyrrhotite ($Fe_{1-x}S$) as "FeS" because the exact stoichiometry and structure is unknown in most instances. A plot of analyses of Wild 2 Fe-Ni sulfides (Fig. 2) shows that many have compositions close to that of FeS, with less than 2 atom % Ni. Only two pentlandite grains have been found. The complete lack of compositions between these (with intermediate solid solution compositions) suggests (but does not require) that FeS and pentlandite condensed as crystalline species (i.e. did not condense as amorphous phases, which later became annealed (19). The remaining Fe-Ni sulfides (approximately half) have compositions that reflect progressive loss of S, as they trend from FeS directly towards the Fe apex. SAED patterns for these S-depleted phases show the presence of two different lattices- strong maxima for a Fe-Ni sulfide phase and a much finer pattern consistent with a metal phase, but which could be an oxide. Loss of S from Fe-Ni sulfides is almost certainly a result of capture heating, and could be used to gauge the degree of capture modification of the enclosing Wild 2 grains. The single verified pentlandite crystal in only one Wild 2 track is intriguing since this phase is frequently an indicator of low-temperature metamorphism under oxidizing conditions, and/or aqueous alteration (20).

A Cu-Fe sulfide, probably cubanite ($CuFe_2S_3$), is present within terminal grains in at least two tracks (22 and 26). Cubanite is occasionally encountered in extraterrestrial materials, most commonly in carbonaceous chondrites. (Fe,Zn)S was found within a terminal grain from Track 22. If it can be established that this phase is in equilibrium with FeS and metal it may be appropriate to apply the sphalerite cosmobarometer to this particular particle (21).

Fe-Ni metal is present as nanoscale beads in significant quantities in most tracks, partly as a product of capture heating of Fe-Ni sulfides, but the high abundance of Ni in these requires that some of this metal is intrinsic to the comet particles. In addition, Tracks 38 and 43 have ~5 μm-sized Fe-Ni metal terminal grains (Ni/Fe~0.03), which appear to be indigenous cometary phases.

Some Wild 2 grains contain alkali-rich mineral assemblages, including phases in Tracks 3 and 16 with compositions corresponding to K-feldspar (SAED patterns suggest a feldspar-like structure, but the exact phase not known) and eifelite ($KNa_2(MgNa)Mg_3Si_{12}O_{30}$) (Track 56). The latter phase identification is based on composition only, and requires further verification. Eifelite is in the osumilite mineral group, whose members have been reported in iron meteorites, as well as enstatite and ordinary chondrites (22), where they formed from a combination of igneous and metasomatic processes. In addition, alkali-rich silicate material is present in some of the larger craters in aluminum foil, but it has not been well characterized.

TEM observations of some tracks revealed the presence of carbonaceous phases. In the terminal grain from tracks 10, 13, 27, 41, 57, 58 there are submicrometer-sized subgrains of poorly-crystalline carbon. Some of these are attached to Fe-Ni sulfides suggesting a genetic relationship.

No evidence of phyllosilicates or indigenous carbonate has been seen in any Wild 2 samples. Despite the fact that significant heating and structural modification accompanied collection of many grains in the aerogel, we would have seen characteristic compositions, grain morphologies, and lattice fringes of phyllosilicates or carbonates had they been present (2, 3, 23). Serpentine and Ca carbonates of the same sizes as in IDPs have been successfully captured in silica aerogel even at velocities 1 km/s higher than those experienced at Wild 2, in both

laboratory simulations and actual IDP collection in Earth orbit aboard the MIR space station. In instances where phyllosilicates have been dehydrated, rendered amorphous, or recrystallized during capture in silica aerogel, characteristic grain morphologies and basal lattice spacings are formed which signal the original mineralogy (2, 23). Thus the lack of these phases among the ~50 Wild 2 grains we have so far well characterized suggests that they could not have composed more than a few percent of the more coarse-grained fraction of captured Wild 2 sample.

Along most tracks are found abundant rounded, glassy silicate bodies containing submicrometer-sized beads of silicates, Fe-Ni sulfides and Fe-Ni metal (Fig. 1c&d). In some respects these bodies are similar to the bits of Glass with Embedded Metal and Sulfides (GEMS) common to most anhydrous chondritic IDPs (5), as well as one peculiar clast in the unequilibrated carbonaceous chondrite Ningqiang (24). It has been proposed that GEMS are among the most primitive of solar system materials, possibly recording the radiation environment of the early Sun or of a presolar environment (5).

The GEMS-like bodies in the tracks often stand out texturally from the typical and dominating aerogel capture medium in terms of composition, structure and morphology. A composition comparison with true GEMS (Table 1) shows similarities but also important differences. For example, compared to the GEMS, the glassy bodies in the tracks have low Fe compared to Mg and S (Table 1). Additionally, there exists a textural difference between GEMS and the Stardust glassy bodies. In GEMS the inclusions are scattered about randomly, and grade from nanometer- to submicrometer-sized objects (5). The glassy bodies in the aerogel tracks have coarser-grained inclusions and a tendency for these to be arranged in non-random patterns. Also, there are sometimes no distinct boundaries between the GEMS-like objects and the embedding aerogel. In addition, some of the metal grains in the Stardust glassy bodies have S-

rich rims, which are not observed in GEMS. Since <5% of GEMS have isotopic compositions very different from terrestrial values (25), we have not been able to determine which, if any, of the glass bodies in the aerogel collectors are cometary "GEMS" and which might be formed as a result of melting and intermingling of fine-grained cometary matter with aerogel during the capture process.

One Wild 2 sample (Track 25) has received special attention (Fig. 4) as it consists of very refractory minerals, including anorthite, a Ca-, Al-, Ti-rich clinopyroxene, gehlenite, spinel, corundum, FeS, V-bearing osbornite ((Ti,V)N), and a phase which is probably perovskite. The osbornite occurs as sub-100nm-sized grains within spinel, and its identification was carefully established by a combination of Electron Energy Loss Spectroscopy (EELS) and SAED work; it may be associated with titanium oxide. The largest terminal grain from Track 25 is ^{16}O rich (26).

Track 25 yielded a terminal particle and at least four major subparticles which have been characterized. These particles exhibit some similarities and some differences with calcium-, aluminum-rich inclusions (CAIs) found in carbonaceous chondrites; in particular they have mineralogies similar to CAIs in CV3 and CM2 chondrites, a significant finding since the inclusions are known to be among the most primitive solar system objects (based on their mineralogy, reduced oxidation state, enrichments in refractory trace elements, isotopes, etc.). In particular they have mineralogical properties similar to CAIs in some carbonaceous chondrites.

Some analyses of pyroxene from the one slice of the Track 25 terminal grain containing gehlenite fall within the range of typical Ti-, Al-rich clinopyroxene from CAIs in CV3 chondrites (e.g. Allende), termed "fassaite" (27); the comparison would be stronger if we could measure the Ti^{3+}/Ti^{4+} ratio of the grain (Fig. S4). Compositions of pyroxenes from subparticles and at least one other slice of the terminal particle, however, do not overlap with Allende

compositions and do not exhibit the interelement covariations seen in meteoritic pyroxenes (Fig. S4). For example, Allende fassaite analyses (28) define clear trends in which MgO is strongly correlated with SiO_2 and anticorrelated with TiO_2. (Fig. S4a&c). The Track 25 pyroxenes do not fall on these trends. The Track 25 pyroxenes have lower CaO contents than meteoritic CAI clinopyroxene, though there is some uncertainty in the interpretation of the analyses of some Wild 2 pyroxene due to possible contamination from adjacent phases, and the extrapolation of analyses from low count rates. Calculations in which possible excess silica (from the aerogel) and spinel (from the sample) components were removed from the Track 25 EDS analyses did not improve the fits to the Allende trends. Also, the Track 25 samples are much finer grained than most meteoritic CAIs, as were the few observed refractory IDPs (29, 30). Overall, due to the differences in pyroxene composition trends, the presence of osbornite, and the apparent low abundance of melilite, the Track 25 sample does not appear to be identical to coarse-grained refractory inclusions from CV3 chondrites.

A better match for the mineralogy of the Track 25 grains would be the spinel-pyroxene inclusions found in CM2 chondrites such as Murchison, CR2 and CH-CB chondrites (31, 32, 33, 34, 35). The CAI in CM chondrites tend to have spinel-rich cores and pyroxene-rich outer regions, which is what the Track 25 subgrains might represent. The pyroxene in them is aluminous and commonly contains Ti. Some spinel-rich inclusions in Murchison contain minor amounts of melilite, as does Track 25. Mg-Al spinel from refractory objects in Murchison is ^{16}O-rich, ~-40‰, but the O-isotopic composition of pyroxene in CM spinel-pyroxene inclusions is not known.

The minerals within the Wild 2 CAI-like particle, especially the osbornite, requires rather high temperatures for formation, possibly higher than 2000K depending on oxygen fugacity (36).

According to equilibrium thermodynamic calculations, osbornite+spinel+Ca-rich clinopyroxene is a stable condensate assemblage in systems otherwise solar in composition only if their atomic C/O lies between ~0.79 and ~0.97, well above the solar value of 0.5. The presence of a CAI-like particle in Comet Wild 2 appears to require large-scale radial transport in the protoplanetary disk (37). Although the anorthite in this particle is too small for a meaningful search for evidence of ^{26}Al, this may prove possible in some refractory Wild 2 grains.

The recovered Wild 2 samples are mixtures of crystalline and amorphous materials. Analytical Electron Microscopy (AEM) analysis of grains from the upper portions of tracks show that they typically have widely varying compositions, sometimes similar to chondrites for most elements except Si, even in severely heated and melted regions (Table 1) (38). The crystalline grains observed among the upper portions of individual tracks are almost always sub-micrometer in grain size. These observations suggest that the materials captured in the upper portions of the tracks are, in general, much finer grained than the material at track termini. AEM of very small craters on the aluminum foil also reveals crystalline olivine, pyroxene and sulfides derived from separate submicrometer components within micrometer-size particles. Analyses of the bulk compositions of tracks by Synchrotron X-Ray Fluorescence (SXRF) (38), suggests that 65-90% of the collected grains' mass is found in upper portions of tracks, and only 10-35% is represented by the track termini grains. However, the SXRF technique probably measures <20% of the mass of most particles that hit since it can't quantify O, C, Si, Mg, and H, because the grains are being analyzed though aerogel. Furthermore, many terminal particles are Fo-rich olivine, which are essentially invisible in the SXRF results. For these reasons the SXRF results cannot be definitive in this matter. Nonetheless, our emerging model for the structure of the captured grains is that many were predominantly very fine-grained (sub-micrometer), loosely-

bound aggregates with a bulk chondritic composition, most also containing much larger individual crystals (most commonly) of olivine, pyroxene and Fe-Ni sulfides. Out of the ~70 tracks we have carefully photodocumented, only 2 appear to have no visible terminal grains which indicates that practically all collected cometary particles contained some of these larger grains. This physical structure is consistent with several chondritic materials, most notably chondritic interplanetary dust particles (12). This structure is also consistent with some of the larger crater morphologies observed on the Stardust Al foils, which have a multilobe appearance rather than being simple hemispherical craters (Fig. S5), and which can contain diverse sub-grain compositions). In general, the captured Wild 2 grains are much finer-grained than the bulk of meteoritic matrix materials or IDPs.

Considering first the ferromagnesian mineral dominated Wild 2 grains, olivine and pyroxene have the same range of Mg, Fe, Mn and Cr compositions as those in anhydrous chondritic IDPs (with the exception of a single Fo5 terminal grain (Fig. 3), and very similar to those in type 2 and some type 3 carbonaceous chondrites. The lack of hydrous phases among the Wild 2 samples precludes a common origin with type 1 or 2 chondrites. The type 3 carbonaceous chondrites (including primitive chondrites Acfer 094 and ALHA 77307) (39, 40) and hydrous chondritic IDPs generally have narrower, or somewhat equilibrated olivine and pyroxene compositional ranges (41). However, with the exception of the two pentlandite grains encountered in our examination, the Fe-Ni sulfide compositions for the Wild 2 grains are similar only to the anhydrous chondritic IDPs. Hydrous IDPs and all chondrites contain large amounts of pentlandite and low-Ni pentlandite (20). In addition, the absence of any identified aqueous alteration products in the Wild 2 grains (no phyllosilicates, indigenous carbonates, etc.) eliminates the hydrous chondritic materials from direct comparison.

No nuclear tracks have yet been observed among Wild 2 samples. It is possible that the majority of these, if ever present, were annealed during capture, although some were observed in crater residue on the Long Duration Exposure Facility, and in lunar silicate grains shot into aerogel (42).

In summary, the bulk of the Wild 2 samples appear to be weakly-constructed mixtures of nanometer-scale grains with occasional much larger (>1μm) ferromagnesian silicates, Fe-Ni sulfides and Fe-Ni metal. The restricted compositional ranges of the sulfides, and very wide range for silicates suggests that Wild 2 experienced little or no aqueous alteration. Of known extraterrestrial materials, the anhydrous chondritic IDPs and anhydrous micrometeorites are most similar to the Wild 2 grains, and in fact a cometary origin for anhydrous IDPs has been suspected for many years (43). The similarity of Wild 2 samples to some IDPs demands re-examination of the latter with new eyes, for there are some apparent differences. For example Fe-Cr-Ti oxides have not been reported as inclusions in IDP olivines, nor has orthoenstatite been reported (12). The very wide ranges of olivine and low-Ca pyroxene compositions in Wild 2 require a wide range of formation conditions, including diverse temperatures and fO_2, probably reflecting different locations in the protoplanetary disk. It is critical to determine the role of annealing in cometary grain formation, but this cannot be assessed with the mineralogic data in hand.

The presence of a refractory particle resembling meteoritic CAI among the Wild 2 grains raises many new questions. IDPs are believed to contain samples of both asteroids and comets and wholly refractory IDPs were identified two decades ago (29, 30), but have received very little attention. In mineralogical terms, the Wild 2 CAI-like particle appears similar to these poorly understood IDPs, and is similar (though finer grained) in various respects to CAI from CM, CR, and CH-CB chondrites.

The lack of aqueous alteration products in Wild 2 samples is in clear contrast to the mineralogy reported for Comet Tempel 1 by the Deep Impact Mission and associated ground-based observers (8). This mineralogical difference could be due to differences in the geological histories of Jupiter-family comets (44).

Acknowledgements

We thank the American public for supporting the Stardust Mission with valuable tax dollars, and our many home institutions and funding agencies for making possible this concentrated 9-month long analytical effort. The dedicated personnel of the JSC Curation Facility were critical to our analytical efforts. We also thank our good friends at Lockheed Martin Space Systems for the wonderful spacecraft. Part of this work at LLNL was performed under the auspices of the U.S. Department of Energy by UC, Lawrence Livermore National Laboratory under contract No. W-7405-Eng-48.

References and Notes

1. R.A. Barrett, M.E. Zolensky, R. Bernhard, *Lunar and Planetary Science,* 24, 65 (1993).

2. F. Hörz, M.E. Zolensky, R.P. Bernhard, T.H. See, J.L. Warren, *Icarus* 147, 559 (2000).

3. M.J. Burchell, G. Graham, A. Kearsley, *Annual Review of Earth and Planetary Sciences* 34, 385 (2006).

4. F. Hörz et al., *Science* This volume.

5. J.P. Bradley, *Science* 265, 925 (1994).

6. E.K. Jessberger, A. Christoforidis, J. Kissel, *Nature* 332, 691 (1988).

7. M.E. Lawler, D.E. Brownlee, S. Temple, M.M. Wheelock, *Icarus* 80, 225 (1989).

8. C. Lisse et al., *Science* 313, 635 (2006).

9. J. Akai, *Proceedings of the NIPR Symposium on Antarctic Meteorites* 3, 55 (1990).

10. M.E. Zolensky, W.H. Kinard, *Advances in Space Research* 13, 75 (1993).

11. W. Klöck, K.L. Thomas, D.S. McKay, H. Palme, *Nature* 339, 126 (1989).

12. F.J.M. Rietmeijer, in *Planetary Materials*, J.J. Papike, Ed., Mineralogical Society of America, 95 (1998).

13. M. Gounelle, B. Devouard, C. Engrand, M. Genge, A. Topani, H. Leroux, *Meteoritics Planetary Science* **37**, A55 (2002).

14. S.B. Simon, L. Grossman, *Meteoritics Planetary Science* 38, 813 (2003).

15. M.K. Weisberg, H.C. Connolly, D.S. Ebel, *Meteoritics and Planetary Science* 39, 1741 (2004).

16. A. Tsuchiyama, *Lunar and Planetary Science Conference XXXVII*, Abstract #2001(2006).

17. W.A. Deer, R.A. Howie J. Zussman, *Rock-Forming Minerals, Volume 2A, Single-Chain Silicates*, Longman Pub. Co. (1978).

18. J. Ganguly, V. Tazzoli, *American Minerlogist* 79, 930 (1994).

19. D. Vaughan, J. Craig, *Mineral Chemistry of Metal Sulfides*. Cambridge Univ. Press., 493 (1978).

20. M.E. Zolensky, K. Thomas, *Geochim. Cosmochim. Acta* 59, 4707 (1995).

21. M.N. Hutchison and S.D. Scott, *Geochim. Cosmochim. Acta* 47, 101 (1983).

22. A.N. Krot, J.T. Wasson, *Meteoritics* 29, 707 (1994).

23. R.A. Barrett, M.E. Zolensky, F. Hörz, D.J. Lindstrom, E.K. Gibson, *Proceedings of the 19th Lunar and Planetary Science Conference*, 22, 203 (1992).

24. M.E. Zolensky et al., *Meteoritics and Planetary Science* 38, 305 (2003).

25. S. Messenger, L.P. Keller, F.J. Stadermann, R.M. Walker,E. Zinner, *Science* 300, 105-108 (2003).

26. K. McKeegan et al., *Science* This Volume.

27. E. Dowty, J.R. Clark , *American Minerlogist* 58, 230 (1973).

28. S.B. Simon, L. Grossman, *Geochimica et Cosmochimica Acta 70*, 780 (2006).

29. M.E. Zolensky, *Science* 237, 1466 (1987).

30. K. McKeegan, *Science* 237, 1468 (1987).

31. G.J. MacPherson, M. Bar-Matthews, T. Tanaka, E. Olsen, L. Grossman, *Geochim. Cosmochim. Acta* 47, 823 (1983).

32. G.J. MacPherson et al., *Proc. 15th Lunar Planet. Sci. Conf., JGR* 89, supplement, C299 (1984).

33. J. Aléon, A.N. Krot, K.D. McKeegan, *Meteoritics Planetary Science* 37, 1729 (2002).

34. M.K. Weisberg, M. Prinz, C.E. Nehru, *Earth and Planetary Science Letters* 91, 19 (1988).

35. A.N. Krot, M. Chaussidon, G.R. Huss, A.A.Ulyanov, M.A. Ivanova M. A., *Meteoritics and Planetary Science* 41, A101 (2006).

36. D. Ebel, in *Meteorites and the Early Solar System II*, D.S. Lauretta and H.Y. McSween Jr., Eds., Univ. Ariz. Press, 253 (2006).

37. F. Shu, H. Shang, A.E Glassgold, T. Lee, *Science* 277, 1475 (1997).

38. G. Flynn et al., *Science* This volume.

39. A.J. Brearley, *Geochim. Cosmochim. Acta* **57**, 1521 (1993).

40. A. Greshake, *Geochim. Cosmochim. Acta* 61, 437 (1997)

41. M.E. Zolensky, R.A. Barrett, *Meteoritics* 29, 616 (1994).

42. P. Tsou et al., *Lunar and Planetary Science Conference XXI*, 1264 (1990).

43. A.O. Nier, D.J. Shlutter, *Meteoritics*, 28, 675 (1993)

44. D.E. Brownlee et al., *Science* This volume.

45. E. Anders and M. Ebihara, *Geochim. Cosmochim. Acta* 46, 2363 (1982). Note: Carbon is ignored in the calculations, and oxygen is calculated.

Table 1: Quantitative EDS analyses (atomic %) of two GEMS-like objects embedded in aerogel of Track 35 (GEMS #1 and 2), compared with actual GEMS in a chondritic IDP and CI abundances.

Element [atom %]	GEMS-like #1 [60 nm diameter]	GEMS-like #2 [100 nm in diameter]		GEMs in IDPs (5)			CI (45)
O	64.95	65.8	65.7	75.3	61.9	56.2	49.7
Mg	6.3	3.5	4.6	1.2	2.9	22.3	10.3
Si	26.4	28.4	26.0	19.1	16.9	13.3	11.5
S	1.75	1.65	2.7	1.2	6.1	3.2	5.7
Ca	0.1	0.1	0.15	Nd	0.15	nd	0.3
Cr	trace	trace	trace	0.2	0.3	0.1	0.3
Mn	0.1	0.1	0.15	0.1	nd	nd	0.2
Fe	0.3	0.2	0.5	2.2	11.1	4.2	20.0
Ni	0.1	0.1	0.2	0.4	nd	0.1	1.1
Al	nd	nd	nd	0.5	0.8	0.6	0.9

Figure Captions

Figure 1. Bright-field TEM images of Wild 2 grains. a: View of the compressed and vesicular, melted aerogel surrounding grains and lining track walls. Dark gray and black objects are admixed silicates, Fe-Ni metal and Fe-Ni sulfides. b: Captured Wild 2 grain composed predominantly of forsterite and troilite, mantled by compressed to melted aerogel. c: Glassy body from Wild 2 track 10 resembling a GEM; rounded dark inclusions are predominantly Fe-Ni metal, Fe-Ni sulfides and ferromagnesian silicates. d: GEM from an anhydrous chondritic IDP; rounded dark inclusions are predominantly Fe-Ni metal, Fe-Ni sulfides and ferromagnesian silicates.

Figure 2. Composition ranges of Fe-Ni sulfides from 6 Wild 2 tracks. Grains from track walls as well as track termini were analyzed. Most Wild 2 sulfides are probably a mixture of troilite and pyrrhotite, and one grain of pentlandite is present. Many sulfides plot with nonstoichiometric, low S compositions reflecting capture heating. The corresponding composition ranges for hydrous and anhydrous chondritic IDPs (20) are also shown. Anhydrous chondritic IDPs contain only troilite and pyrrhotite, while the hydrous chondritic IDPs also have equally-abundant Ni-rich sulfides including pentlandite. With the exception of the single pentlandite crystal, the Wild 2 grains have the same Fe-Ni sulfide composition range as the anhydrous chondritic IDPs.

Figure 3. Composition ranges of olivine (Fo) and low-calcium pyroxene (En) from 10 Wild 2 grains (tracks). Grains from track walls as well as track termini were analyzed, but predominantly the latter. The corresponding composition ranges for hydrous and anhydrous

chondritic IDPs are also shown (41). The Wild 2 grains have the same olivine and low-calcium pyroxene composition ranges as the anhydrous chondritic IDPs, although the presence of mixed hydrous and anhydrous materials is compatible with these data.

Figure 4. The Track 25 CAI-like grain. a: BSE image of the CAI-like grain from Track 25, showing the grey shell of compressed and compressed to melted aerogel at lower left. b: EELS element maps of an orbornite grain – BSE, N, Ti and V. c: EELS spectrum of an osbornite grain showing peaks for N, TI and V. d: SAED pattern of osbornite; the phase is crystalline, and the lattice spacings are indeed consistent with osbornite.

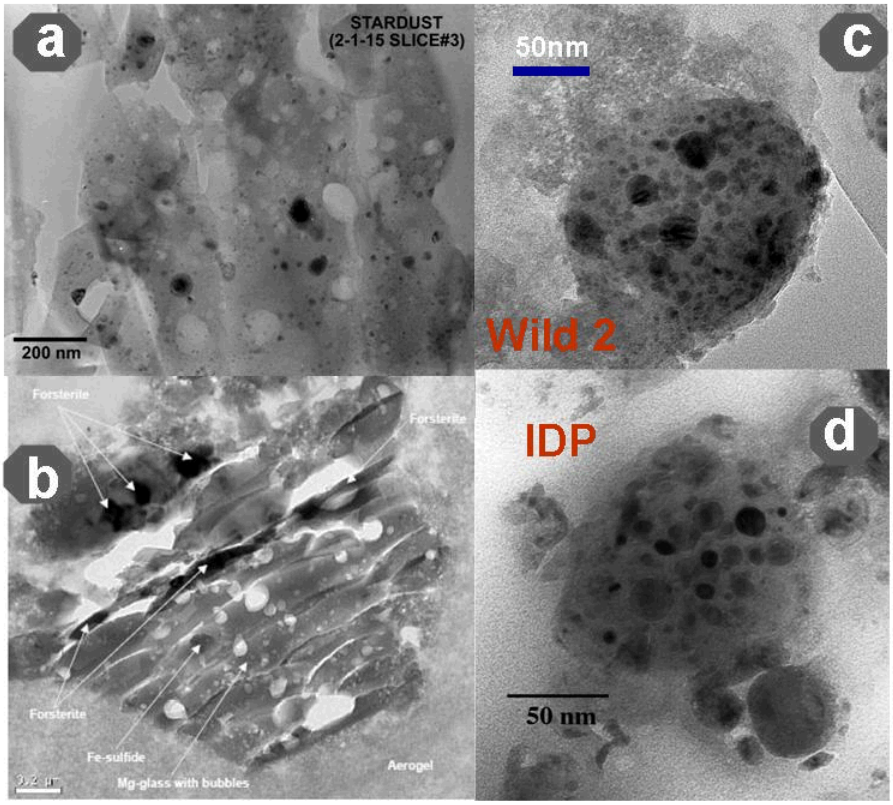
a
STARDUST
(2-1-15 SLICE#3)
200 nm
c
50nm
Wild 2
b
Forsterite
Forsterite
Forsterite
Fe-sulfide
Mg-glass with bubbles
Aerogel
d
IDP
50 nm

Figure 1

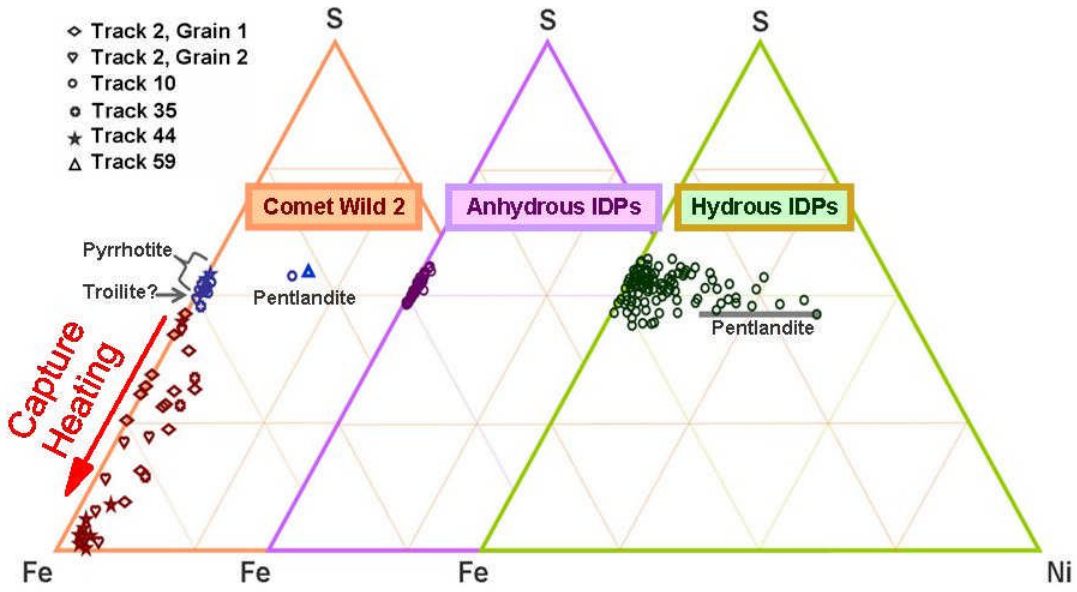
Track 2, Grain 1
Track 2, Grain 2
Track 10
Track 35
Track 44
Track 59
S
S
S
Comet Wild 2
Anhydrous IDPs
Hydrous IDPs
Pyrrhotite
Troilite?
Pentlandite
Pentlandite
Capture
Heating
Fe
Fe
Fe
Ni

Figure 2

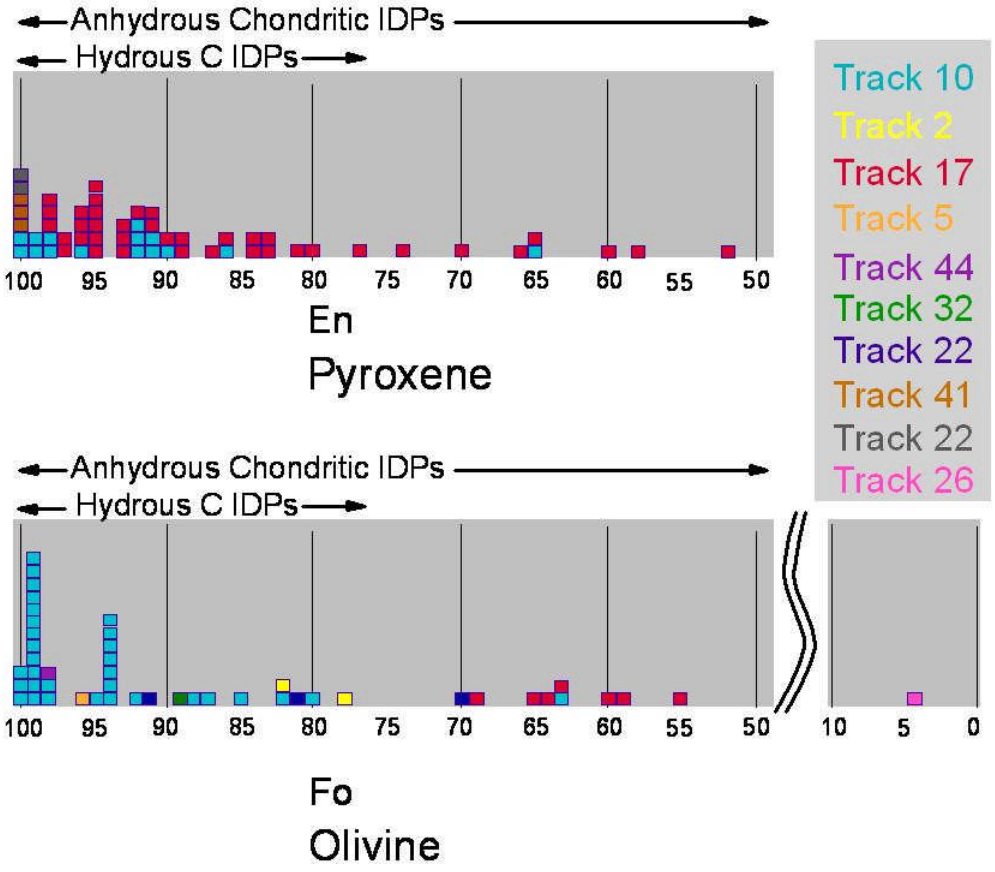
Anhydrous Chondritic IDPs
Hydrous C IDPs
100 95 90 85 80 75 70 65 60 55 50
En
Pyroxene
Track 10
Track 2
Track 17
Track 5
Track 44
Track 32
Track 22
Track 41
Track 22
Track 26
Anhydrous Chondritic IDPs
Hydrous C IDPs
100 95 90 85 80 75 70 65 60 55 50 10 5 0
Fo
Olivine

Figure 3

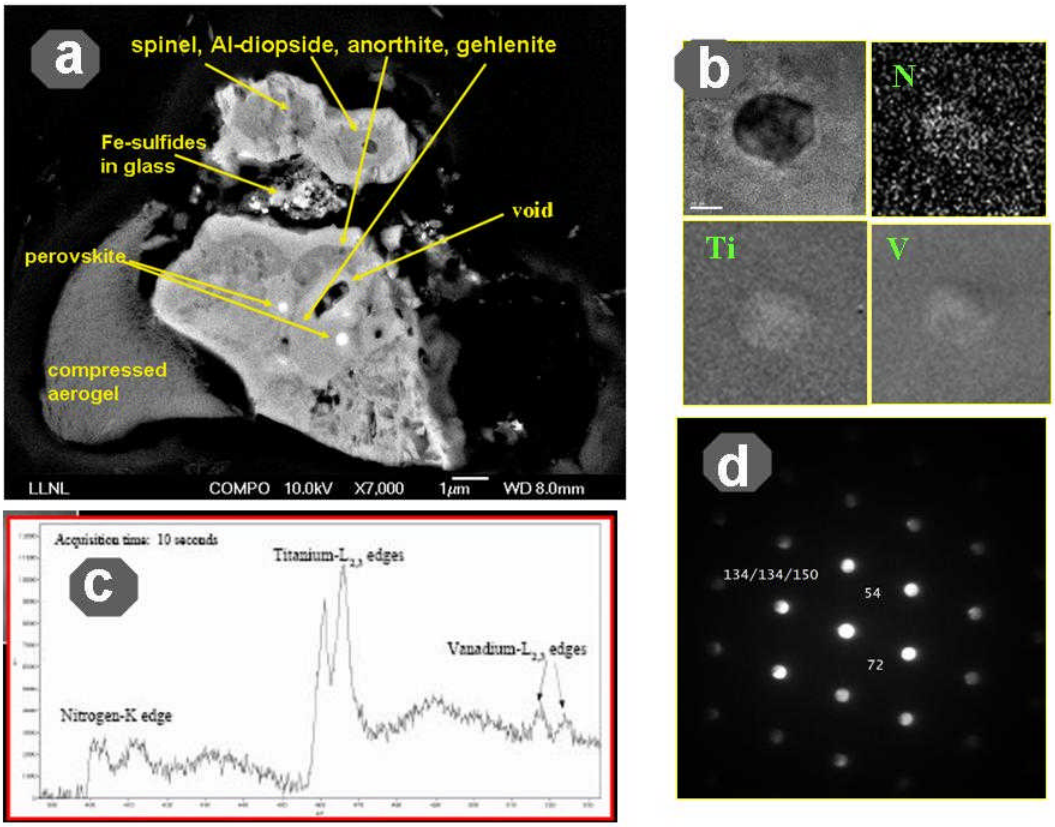
a
spinel, Al-diopside, anorthite, gehlenite
Fe-sulfides in glass
void
perovskite
compressed aerogel
LLNL
COMPO 10.0kV X7,000 1μm WD 8.0mm
b
N
Ti
V
c
Acquisition time: 10 seconds
Titanium-L2,3 edges
Vanadium-L2,3 edges
Nitrogen-K edge
d
134/134/150
54
72

Figure 4

Supporting Online Materials

Techniques

To remove grains from aerogel we used a combination of old and new techniques. For larger features we could use straight razor blades to trim away excess aerogel. For the bulk of tracks however, we mainly used two newly-developed techniques: keystoning and quikstoning (Fig. S6).

Whole tracks in the aerogel collectors were extracted using the keystoning technique developed at the Space Sciences Laboratory, U. C. Berkeley (1). Glass rods (1mm diameter) are pulled to make two microneedles. The needles are held by micromanipulators which are attached to the stage of the extraction microscope. The needles cut the aerogel by repetitive "poking". The micromanipulators are driven automatically by computer. First, an angled cut is made which undercuts the deepest feature of a particular impact; then a vertical cut is made around the impact. The resulting wedge-shaped block of aerogel (a "keystone") contains the entire impact track and the terminal particles. The keystone is then removed from the collector using silicon microforks which are inserted into pre-machined holes in the keystone. For certain analytical techniques, it is desirable to slice a track into multiple cross-sections; other techniques require a sample of the bulb that has been cleaved lengthwise. These specialized samples are prepared by laying a keystone on its side and using the same aerogel cutting tools to dissect or slice wafers of the track bulb. Some analyses can be made of grains still enclosed in a suitably small keystone, for example synchrotron X-ray diffraction (XRD) and X-ray fluorescence (XRF). When it is time to extract grains from the keystone it can be flattened between two sheets of mylar, and the grains can be easily separated. The flattened keystone preserves the general

positions of the enclosed grains, permitting surveys to be made of mineralogical variation down tracks. For Stardust samples, we made keystones at University of California, Berkeley, and at the NASA Johnson Space Center (JSC).

In quikstoning, a diamond, steel or sapphire utility-knife-shaped blade is driven through the aerogel at ultrasonic frequencies. This micro-blade is controlled by a micromanipulator for fine motion control. The ultrasonic oscillations are generated by the piezo-driver of a MicroDissector (Eppendorf) which is mounted on the micromanipulator. Details of the instrument are given in (2). Quikstoning was performed at the Lawrence Livermore National Lab and NASA JSC.

The embedding media for Wild 2 grains were EMBED-812 epoxy, sulfur and WELD-ON 40 acrylic. We most frequently used acrylic to mount grains for ultramicrotomy. Particles could then be easily removed from the embedding medium using common organic solvents, including acetone or chloroform, permitting subsequent isotopic or bulk compositional analyses. One problem we encountered was that acrylic polymerized in an electron beam, making subsequent grain removal difficult. We embedded pieces of aerogel in EMBED-812 epoxy, during which the aerogel became completely invisible, revealing all of the grains in a track in the most complete manner (3). When it was desirable to make superior organic analyses of grains following ultramicrotomy we used sulfur as the embedding medium, as had been the standard practice for IDPs and fine-grained chondritic meteorites.

Comet Wild 2 grains were also embedded in high-purity S and sliced into 50~ 70 nm-thick sections with an ultramicrotome equipped with a diamond knife. The sections were floated onto ultra-pure water and transferred to amorphous C-supported Cu Transmission Electron Microscopy (TEM) grids. The S was sublimed prior to analysis focused on organic matter in the

sample such as C- and N- X-ray Absorption Near-Edge Structure (XANES), Fourier Transform Infra-Red spectroscopy (FTIR) and light element isotopic analysis in the Nano- Secondary Ion Mass Spectrometer (NanoSIMS). Sulfur was chosen as an embedding medium to avoid contamination of the samples with low viscosity resin (epoxy) normally used for ultramicrotomy. Sulfur beads containing the samples were attached to a sample holding bullet using cyanoacrylate. To evaluate the potential glue contribution to the sample analysis, sulfur beads devoid of sample were prepared in the same manner. We did not see any evidence that cyanoacrylate penetrated the S bead during subsequent TEM investigation of the sample-free S slices. Electron Energy-Loss Spectroscopy (EELS) spectra acquired from the S test slices also did not show evidence of the pronounced CN peak characteristic of cyanoacrylate.

Micro-FTIR was used to provide a rapid, non-destructive pre-characterization of most grains removed from the aerogel at JSC. This technique was most valuable for terminal grains, which typically contained crystals larger than 1 um. However, FTIR generally failed to locate crystalline material within finer-grained particles, especially those from the upper portions (including bulbs) of tracks.

For Synchrotron X-ray Powder Diffraction (SXRF) each stardust particle was mounted on a thin glass fiber with a 3 μm thickness using a small amount acetone-soluble bond, set in a Gandolfi camera, and exposed to synchrotron X-rays with a wave length of 2.161 ± 0.001 Å for 3 hours to produce a powder X-ray diffraction pattern. The analysis was performed at beam line 4A of the Photon Factory, Institute of Material Science, High Energy Accelerator Research Organization and at beam line 37XU of the Japan Synchrotron Radiation Research Institute (SPring 8).

The TEM results reported have been obtained at many institutions. In Lille we used a Philips CM30 (LaB6 filament, working at 300 keV) and a Tecnai G2-20 twin (LaB6 filament, 200 kV). Structural (diffraction) data were obtained using the Selected Area Electron Diffraction (SAED) technique. Chemical compositions were measured using Energy Dispersion X-ray Spectroscopy (EDX) Noran and EDX Si-detectors (CM30 and Tecnai, respectively). Correction procedures have been applied (k-factors and absorption corrections).

At Michigan State University we used a JEOL 6400 Scanning Electron Microscope (SEM) operated at 25kV, with a Noran EDX system. TEM work here performed using JEOL 2200FS Field Emission Gun (FEG) TEM at 200kV, with an Oxford EDX system.

At Kobe University grains were studied using a TEM (JEOL JEM-2010) operated at 200 kV and equipped with an EDX detector For quantitative TEM analyses, k-factors for the major elements were determined using standards of San Carlos olivine, San Carlos clinopyroxene, and K-feldspar from Koryu mine, Hokkaido, Japan.

At Friedrich-Schiller-University Jena we used an energy-filtered 200 kV ZEISS LEO922 TEM with a ThermoNoran Six EDX system.

At the University of Chicago, samples were examined with a JEOL JSM-5800 low voltage SEM equipped with an Oxford/Link ISIS-300 EDX system. We also used a Tecnai F30 TEM, with a point-to-point resolution of 0.2 nm, operated at 300 kV.

At the University of New Mexico all STARDUST analyses were performed using a JEOL GEM2010 High Resolution TEM with point-to-point resolution of 0.19 nm. It is equipped with a LINK ISIS EDX system for in situ element analyses with a 5 nm probe. The spectrometer is fitted with an ultrathin window for quantitative light element analyses. The instrument operated at a 200keV accelerating voltage. Additional analyses were performed using a JEOL

2010F FASTEM TEM/STEM instrument operating at 197 keV. The instrument is equipped with a GATAN GIF 2000 imaging filtering system and Oxford INCA/Isis EDS system. The Cliff-Lorimer thin-film procedure was used for quantitative chemical determination with an error <10% (relative). Crystallographic data were obtained by SAED. An LN2-cooled cold-finger was used to minimize sample degradation. Each sample was placed in low-background double-tilt sample holder that was dedicated to this particular project to avoid contact with extraneous materials. All sample handling occurred inside a laminar flow bench.

At the Naval Research Lab TEM analyses were performed using a JEOL 2200FS 200 kV field-emission microscope equipped with a Noran System Six EDX and Gatan Ultrascan Charge-Coupled Device (CCD).

At Tokyo University we used a Hitachi S-4500 FEG-SEM with EDX and Electron Back-Scattered Diffraction (EBSD). We also used a JEOL JEM2010 TEM with an EDX system.

TEM measurements at NASA Johnson Space Center were obtained using a JEOL 2500SE 200kV FEG-STEM equipped with a Noran thin window EDX spectrometer, a Gatan Tridiem imaging filter for Energy-Filtered TEM imaging (EFTEM) and EELS, and a 2K x 2K slow scan CCD camera for recording images. Image acquisition and processing were carried out using Gatan Digital Micrograph software. EFTEM images were collected with acquisition times of 20-60 s depending on element concentrations. EELS spectra were obtained in image mode with spot sizes of 10-50 nm, a dispersion of 0.3 eV, dwell times of 10-30 s at an energy resolution of 0.9 eV full width half maximum at the zero-loss peak. High resolution brightfield images were recorded at 500K-1M X magnification and ordering was estimated using fast Fourier transforms of selected regions within the images.

Time-of-Flight Secondary Ion Mass Spectrometry (TOF-SIMS) was used to obtain lateral element distributions of eight particles sectioned in epoxy as well as two tracks on dissected aerogel keystones. A TOF-SIMS IV instrument from ION-TOF was used in this study. TOF-SIMS allows a comprehensive analysis of elements, isotopes, and molecules at high lateral resolution and minute sample consumption. During a typical TOF-SIMS analysis, less than one atomic monolayer is consumed while the sample is bombarded with a pulsed 25 keV Ga^+ primary ion beam for several hours. This beam with a diameter of ~0.2 μm is rastered over the sample to obtain information on the lateral distribution of the various elements, isotopes, and molecules. All secondary ions of a single polarity are detected quasi simultaneously after their passage through the time-of-flight spectrometer. Both polarities are measured in two consecutive analyses. Further details on the TOF-SIMS technique are given in the literature (4).

The MicroXANES work was performed at beamline ID22 of the ESRF synchrotron in Grenoble, France. The keystones were prepared for synchrotron measurements by being held between 2 thin ultralene sheets (3 microns) in slide-holders. The sharp focus of the microscope resulted in a calibrated and aligned X-ray focused beam 1 x 2 micrometers in size. Beam energy was variable from 6.5 to 20 keV, allowing us to resonantly scan edges of elements Z=25 to 42, or to map out all elements using either K or L lines. Sensitivity of the setup allowed element mapping down to 1 ppm concentration.

Sample Modification and Contamination

All of the Wild 2 particles we have thus far examined have been modified, both physically and mineralogically, to various degrees by the capture process. All particles that may have been loose aggregates, “traveling sand piles”, disaggregated into individual components

with the denser components penetrating more deeply into the aerogel. Individual grains experienced a wide range of heating effects that range from excellent preservation to melting and total dissolution in >1200˚C molten aerogel. (Fig. 1). As a result of this heating many Fe-Ni sulfides have been melted (requiring ~1000˚C, ignoring pressure effects) (5), have lost S due to partial evaporation, and are scattered among the Wild 2 samples as fine Fe-Ni-S beads with non-stoichiometric compositions, often intimately mixed with Fe-Ni metal. Such behavior was expected from our previous experience with silica aerogel and metals both in the laboratory and in actual use in low-Earth orbit (3, 6, 7). The presence of these beads is an indicator that a particular component has been severely heated. What is remarkable is the extreme variability of these modifications and the fact that severely modified and unmodified materials can be found within a micrometer of each other, requiring tremendous local temperature gradients. Within a single captured grain we can observe places where Fe-Ni sulfides have melted, partially devolatilized (loss of S), and mixed with Fe-Ni metal, whereas in other places we see survival of rather delicate Fe-Ni sulfide crystals. A fundamental problem is recognizing the modified grains for what they were prior to impact – discriminating between severely modified and relatively pristine mineral assemblages. Micro-XANES shows that at the beginning of Track 59, sulfate is present as well as an almost neutral S compound, which we believe to have formed during capture heating of sulfides.

Fortunately, we have an internal gauge of heating during collection. Fe-Ni sulfides are ubiquitous in the Wild 2 samples, are very sensitive indicators of heating, and accurate compositional analyses can reveal which have lost S, and which have not (and are therefore stoichiometric) (see Fig. 2a).

One unfortunate result of the fine-scale mixing of the Wild 2 grains with silica aerogel is that it is very difficult to obtain precise analyses for Si smaller than the thickness of ultramicrotomed sections, and any indigenous amorphous cometary materials are now hard to recognize amongst very abundant amorphous silica aerogel and melted cometary minerals. Any indigenous stoichiometric cometary materials are also so mixed, making their identification by purely chemical means very, very difficult. This is partially compensated by materials captured on the aluminum foils, where elemental ratios to Si can be measured, although these residues have undergone even higher pressure and temperature processing than in the aerogel.

Our initial hypothesis was that the degree of captured particle modification would vary considerably along each capture track, with the most modified material being present along the walls of the upper reaches of tracks, and the least modified situated at track termini. To test this idea we analyzed multiple (up to 53) grains from each of three long tracks (all exceeding 1 cm in length). The results for the track with the most complete results are shown in Fig. S1. It is clear that crystalline grains are found along the entire track, not just at the terminus. While it is true that grains at track termini are generally dominated by crystalline material, these terminal grains are sometimes found to be large monomineralic fragments (sometimes single crystals) which have been fractured, disaggregated and thoroughly mixed with aerogel during capture. Because of this mixing, attempts to prepare samples by focused ion beams (FIBing) sometimes come to grief. While grains from the upper reaches of the tracks are universally disaggregated to some degree, many are dominated by materials that are still crystalline, including delicate Fe-Ni sulfides. Some terminal grains are found to be very fine-grained and polymineralic. Therefore one cannot sample a particular segment of any track with the certain expectation of finding only

melted grains. Each track is different, and most contain unmelted samples along their entire length.

Several mineralogic contaminants have been introduced to the samples from trace impurities in the silica aerogel itself. These include materials from the aerogel manufacture process, handling before and during insertion into the Stardust grid, removal from the grid following flight, and sample removal from the aerogel cell. In addition, some of the earliest sample characterization work was performed on chips of aerogel found loose inside the Stardust canister immediately upon opening in the JSC Stardust clean room and were thus subject to additional contamination sources.

One such contaminant is calcite, present as sub-micrometer anhedral to euhedral grains with a composition, determined by STEM-EDX analyses, of pure $CaCO_3$, and the calcite structure confirmed by SAED patterns. These contaminants can usually be easily recognized as such by their occurrence external to the Wild 2 grains, situated instead in the enclosing shells of compressed to melted aerogel. Calcite has been found principally in the loose chips of aerogel recovered from inside of the canister, where contamination opportunities were greatest. Given the importance of carbonates, this is a very unfortunate contaminant, but with careful observation it can be recognized easily as such and be discounted.

A more perplexing material is titanium oxide, usually present here as submicrometer-sized crystallites of brookite (TiO_2), but occasionally occurring as other titania phases, and sometimes containing Al_2O_3 and or Zr_2O_3. These materials usually found surrounding the Wild 2 grains, in enclosing aerogel, and also occasionally lying within the grains. It is therefore possible that a fraction of this material is indeed indigenous to the cometary material. However, these phases are common whitening agents in papers and spacecraft thermal control paints (8)

(though on the Stardust spacecraft none of these paints were in the line of sight of the aerogel), and their presence among the Wild 2 samples is a problem left to future resolution.

These minor exceptions aside, we found very limited contamination from the spacecraft in the aerogel. Potential problems with secondary impacts (cometary grains impacting on the spacecraft, ricocheting and splashing onto the aerogel) failed to materialize. Based on our experience, future missions should be able to avoid this problem almost entirely.

References and Notes

1. A.J. Westphal et al., *Meteoritics & Planetary Science* 39, 1375 (2004).

2. H.A. Ishii, G.A. Graham, A.T. Kearsley, P.G. Grant, C.J. Snead, J.P. Bradley, *MAPS* 40, 1741(2005).

3. R.A. Barrett, M.E. Zolensky, F. Hörz, D.J. Lindstrom, E.K. Gibson, *Proceedings of the 19th Lunar and Planetary Science Conference*, 22, 203 (1992).

4. T. Stephan, *Planet. Space Sci.* 49, 859 (2001).

5. D. Vaughan, J. Craig, *Mineral Chemistry of Metal Sulfides*. Cambridge Univ. Press., 493 (1978).

6. F. Hörz, M.E. Zolensky, R.P. Bernhard, T.H. See, J.L. Warren, *Icarus* 147, 559 (2000).

7. M.J. Burchell, G. Graham, A. Kearsley, *Annual Review of Earth and Planetary Sciences* 34, 385 (2006).

8. M.E. Zolensky, D. S. McKay, L. A. Kaczor *Journal of Geophysical Research* 94, D1, 1047 (1989).

9. S.B. Simon, L. Grossman, *Meteoritics Planetary Science* 38, 813 (2003).

10. W. Klöck, K.L. Thomas, D.S. McKay, H. Palme, *Nature* 339, 126 (1989).

11. S.B.Simon et al., *Geochimica et Cosmochimica Acta* 55, 2635 (1991).

12. S.B.Simon et al., *Geochimica et Cosmochimica Acta* 63, 1233, (1999).

13. S.B. Simon, L. Grossman, *Geochimica et Cosmochimica Acta 70*, 780 (2006).

Supplementary Figures

Figure S1. Results of crystallographic analyses of 14 grains removed from the length of Track 25, which is 11.7 mm long, and is shown here in transmitted light. The cometary particle entered the aerogel at the right, and traveled to the left. The location of predominantly crystalline fragments

are indicated as “C”, those that are entirely amorphous are “A”. It is clear that crystalline fragments are located along most of the track.

Figure S2. a: Cr and b: Mn contents of Wild 2 olivine compared with those in chondritic meteorites, including chondrules, polycrystalline aggregates (polyxt Ol), CM, CI and Tagish Lake (TL) single crystals (9). Also shown is the MnO content of olivine in chondritic IDPs (10). The analyses done thus far suggest that the composition field of the Wild 2 olivine is basically similar to all of these materials for the minor elements Mn and Cr.

Figure S3. Bright field TEM image of abundant Fe-Ni sulfides scattered among low-Ca pyroxene and amorphous silicate material in the terminal grain from Track 17.

Figure S4. Figure Z. Compositional trends of fassaite in Allende CAIs compared with that for the Wild 2 Track 25 CAI-like grain, in terms of cations per six oxygen anions. a: Mg vs. Ti. Track 25 grains have a much weaker anticorrelation than the Allende fassaite. b: Al vs. Si. Track 25 grains have an anticorrelation like that of the Allende fassaite, but generally with a higher Al/Si ratio. c: Mg vs. Si. Track 25 grains do not exhibit the same correlation as the Allende fassaite. Allende data from (11, 12, 13).

Figure S5. (a) Secondary electron image of a complex crater preserved in foil C2029W,1. The crater contains several mass centers suggesting the original cometary projectile was aggregated. (b) A depth gradient map for the crater. (c&d) Composite energy-dispersive X-ray elemental

maps showing the distribution of the different remnant mineral phases preserved in the crater (e.g. silicate and sulfide).

Figure S6. Two particle extraction techniques developed for aerogel. a: Side view of a complete cometary aerogel cell, containing numerous tracks. Outlines indicate the location of a keystone and quikstone to be removed. b: Triangular keystone, removed from aerogel with a track visible within. This keystone measures approximately 3 mm in length. c: Quikstone parallelepiped containing a large bulb-type track. The track measures approximately 1 cm in length.

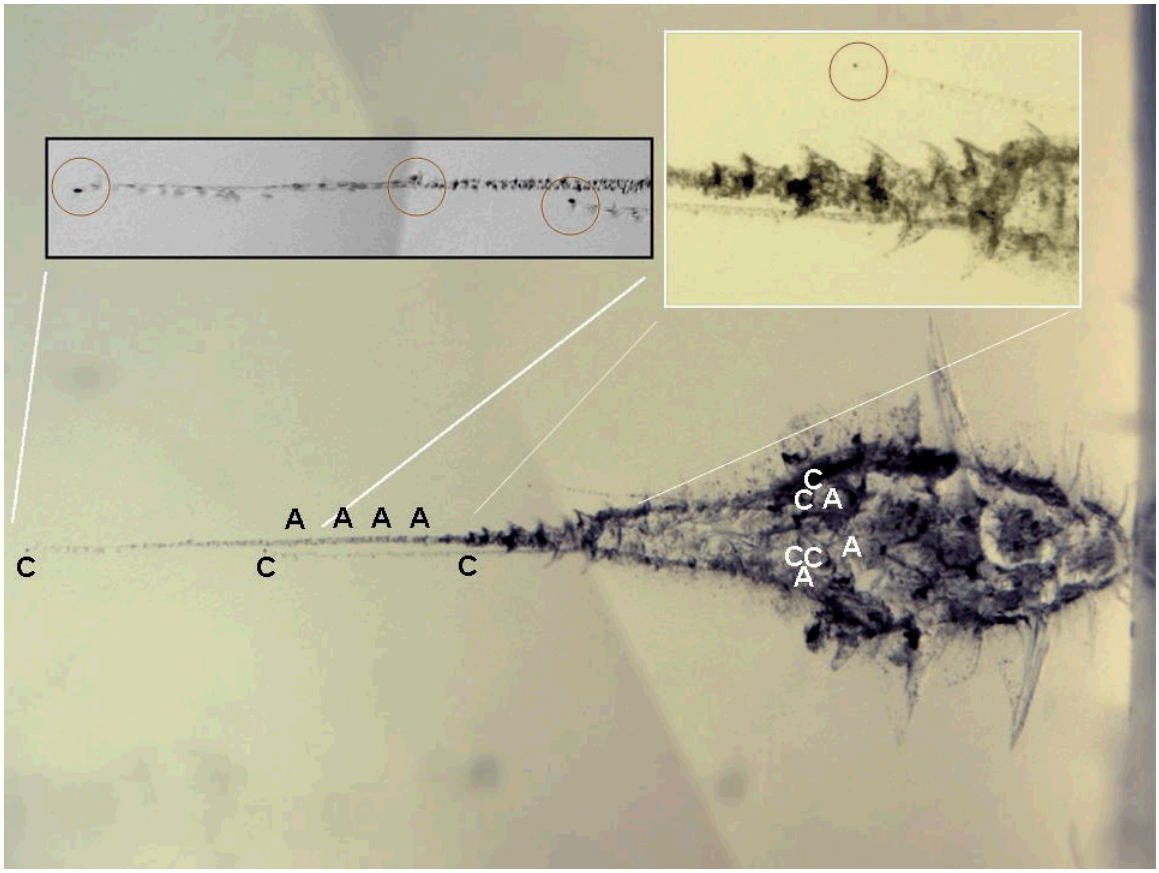

Figure S1

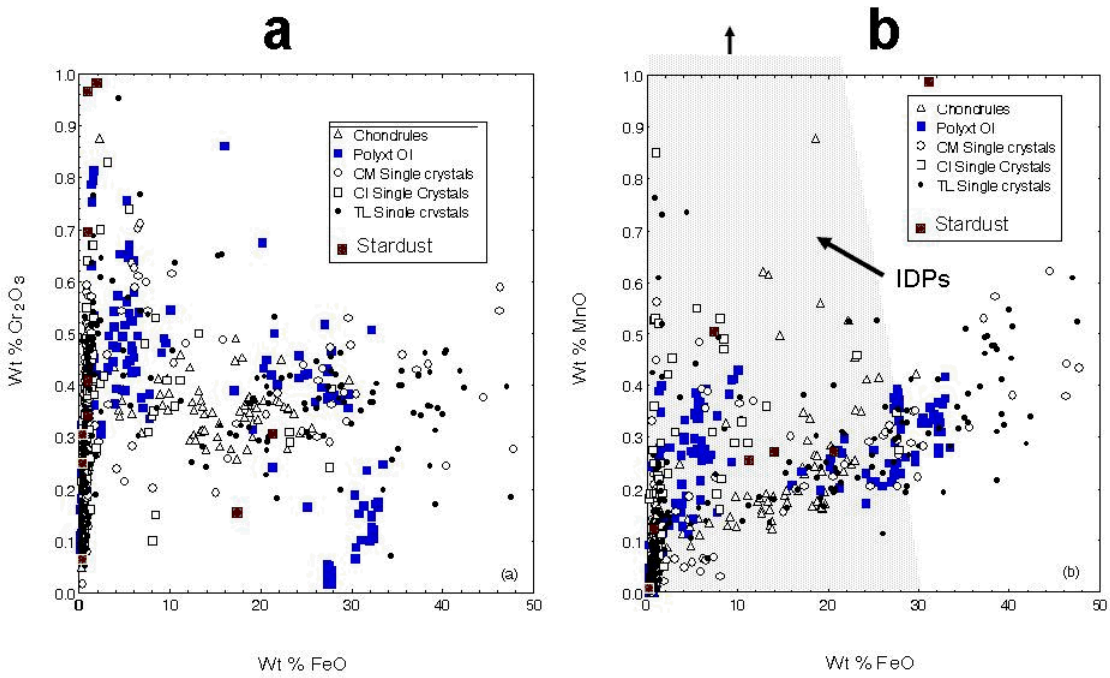
a
b
Chondrules
Polyxt Ol
CM Single crystals
CI Single Crystals
TL Single crystals
Stardust
IDPs
Wt % Cr2O3
Wt % MnO
Wt % FeO
Wt % FeO
(a)
(b)

Figure S2

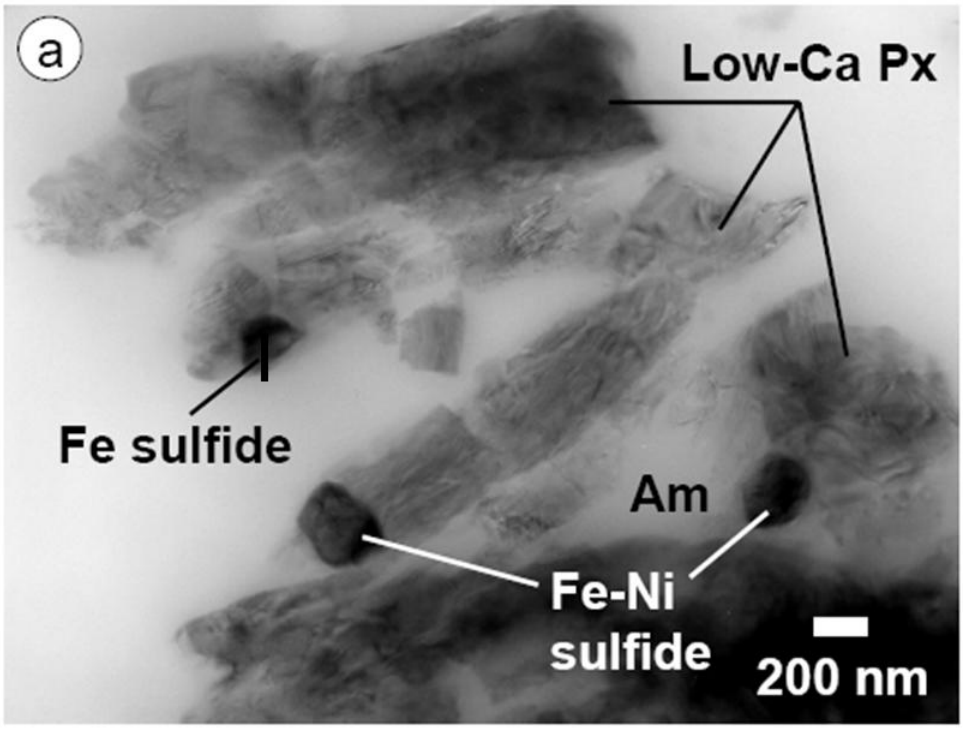

Figure S3

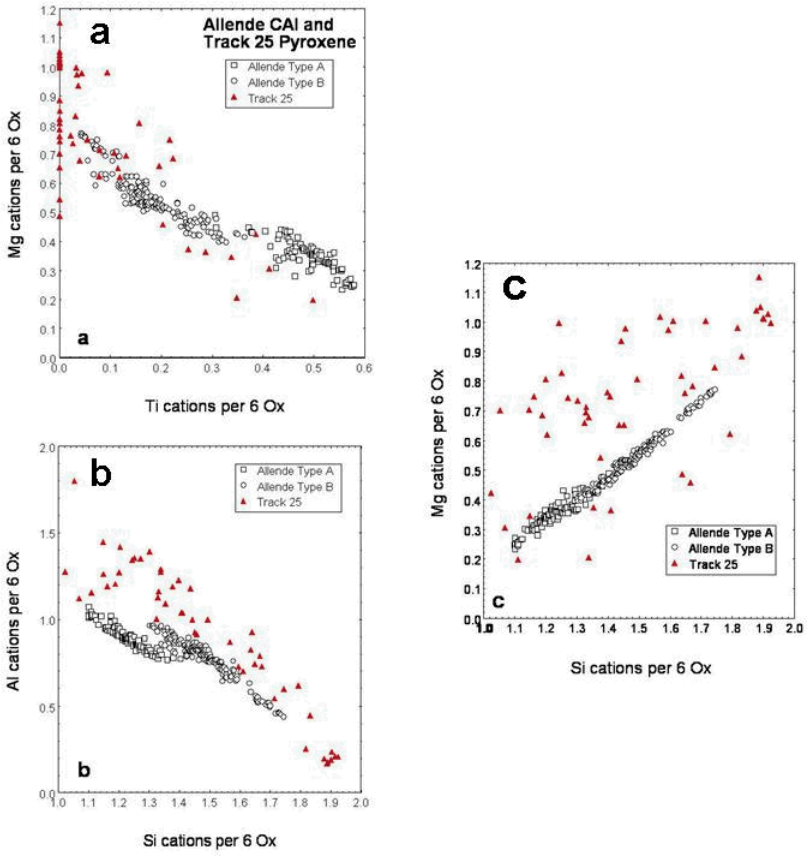
a
Allende CAI and
Track 25 Pyroxene
Allende Type A
Allende Type B
Track 25
Mg cations per 6 Ox
Ti cations per 6 Ox
b
Al cations per 6 Ox
Si cations per 6 Ox
c
Mg cations per 6 Ox
Si cations per 6 Ox

Figure S4

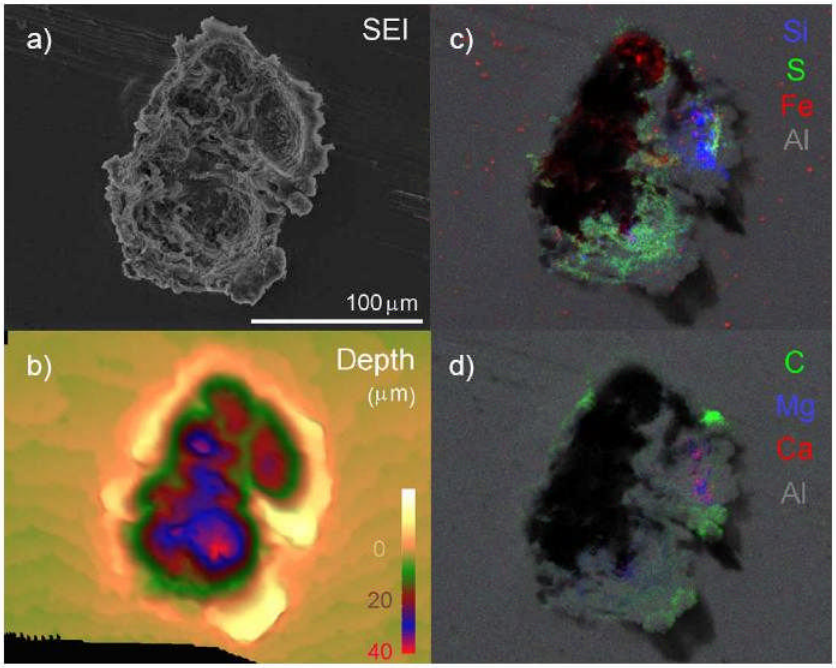

Figure S5

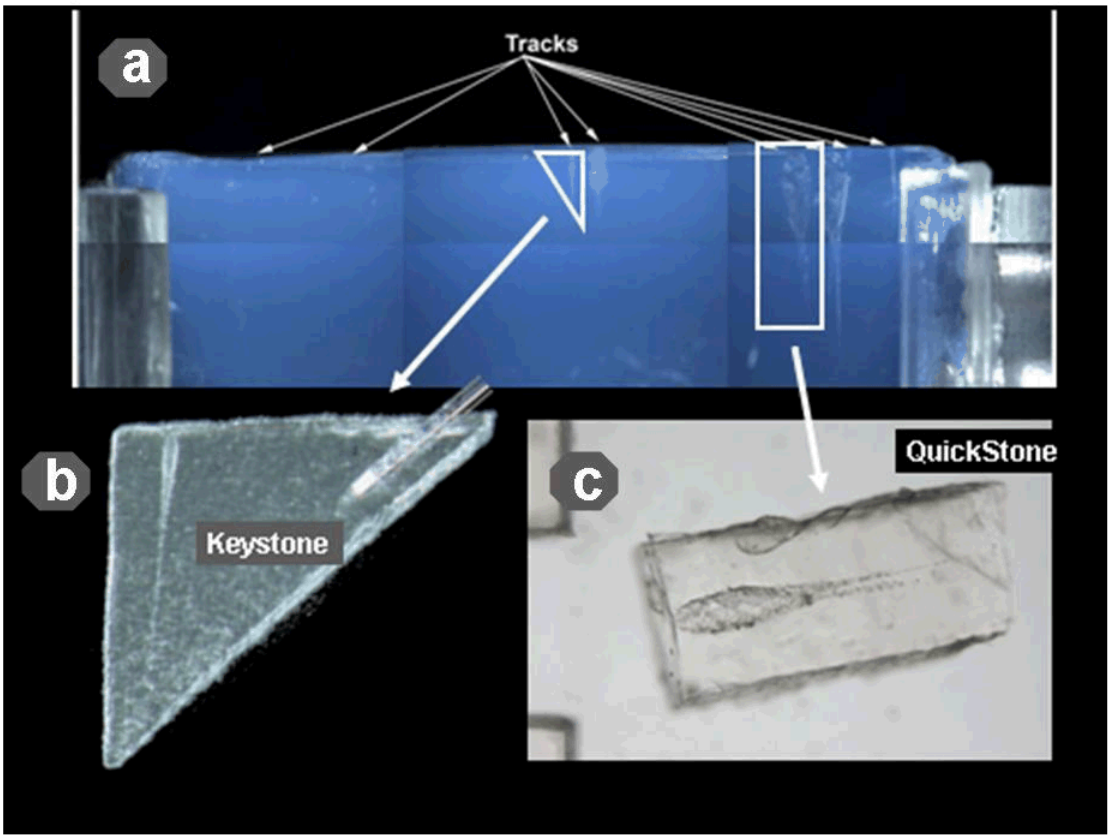

Figure S6